DEUTSCHES ELEKTRONEN-SYNCHROTRON DESY

DESY SR-79/04
March 1979

DETERMINATION OF BOND LENGTHS FROM EXAFS WITH HIGH RESOLUTION

by

Peter Rabe
Institut für Experimentalphysik der Universität Kiel

NOTKESTRASSE 85 · 2 HAMBURG 52

To be sure that your preprints are promptly included in the
HIGH ENERGY PHYSICS INDEX ,
send them to the following address (if possible by air mail) :

DESY
Bibliothek
Notkestrasse 85
2 Hamburg 52
Germany

Determination of bond lengths from EXAFS with high resolution

Peter Rabe

Institut für Experimentalphysik, Universität Kiel, Kiel, Germany

to be published in Jap. I. Appl. Phys.

Abstract

The investigation of EXAFS has grown to an important tool for the analysis of the local geometrical structure in complex systems. The development of the method has been stimulated by the availability of high intensity X-ray sources. Improved techniques of data evaluation are reviewed which permit accuracies for bond lengths better than 0.001 nm.

1. Introduction

The extended X-ray absorption fine structure (EXAFS) showing up above the absorption edges in polyatomic systems has been studied since the thirties[1]. The interest in EXAFS is growing since the usefulness of this fine structure for structural analysis has been demonstrated[2,3]. EXAFS is well known to be an interference phenomenon[4-6]. Photoelectrons produced by the absorption of photons are scattered by the nearest neighbours of the absorbing atom. The superposition of outgoing and backscattered waves produces oscillations in the matrix element of the transition probability. Periodicity and amplitude of these oscillations are determined by the parameters of the local ordering around the central atom, i.e. bond lengths and coordination numbers.

Structural analysis by means of EXAFS has been performed on a wide range of polyatomic molecules[7-10], solutions[11-14], as well as amorphous[15-22] and crystalline[23-27] solids. EXAFS oscillations have also been observed in X-ray fluorescence[28], ultraviolet luminescence[29], Auger electron emission[30], and total photoelectron yield[31] as a function of the photon energy. These alternative techniques open new ways of studying highly dilute materials as biological systems or adsorbates on surfaces[32].

In the following chapter the experimental facilities are described which provide high accuracy absorption data. In chapter 3 alternative techniques to extract bond lengths from

experimental data are reviewed briefly. The improvement of spatial resolution by utilizing the beating in EXAFS caused by the superposition of contributions from close lying shells of scattering atoms is discussed in chapter 4. Finally the consequences of non-symmetric pairdistribution functions for the structural analysis are outlined in chapter 5.

2. Experimental conditions

One of the major improvements in the experimental conditions turned out to be the use of high energy electron accelerators as high brilliancy X-ray sources. Figure 1 shows a comparison of the intensities of the bremsstrahlung and K_α lines of an X-ray tube with copper anode (45 kV, 50 mA, 20° take off angle) (dashed lines) with the synchrotronradiation (SR) of the Deutsches Elektronen-Synchrotron at 10 mA electron current (solid lines). For the X-ray tube the usable solid angle has been taken as parameter. The lowest two dashed lines represent typical intensities available with flat crystal monochromators. The SR intensity at various electron energies is shown for an exit slit of 10 mm height and 0.7 mm width at a distance of 40 m from the tangent point. The horizontal and vertical electron beam size has been taken to be 10 mm and 1 mm respectively. This leads to a total divergence of 0.28 x 0.26 $mrad^2$ (vertical and horizontal). Figure 1 shows that at sufficient high electron energies the intensity of the SR surmounts that of the bremsstrahlung by several orders of magnitude.

Several experimental improvements to gain intensity are possible with both sources. At electron accelerators focussing premirrors allow the collection of larger solid angles. A gain of one order of magnitude in the total intensity available at the experiment together with gain of two orders of magnitude in brightness have been obtained at the Stanford Synchrotron Radiation Laboratory[33]. On the other hand the available intensity of X-ray tubes can be increased by using focusing X-ray monochromators. "Synchrotron like" intensities with a conventional tube have been reported[34]. A further gain of at least an order of magnitude can be made by the utilization of multichannel detectors. Optical multichannel analyzers are widely used in the visible or near ultraviolet region. Together with thin film scintillators these detectors could be used in the X-ray region.

The experimental setup for EXAFS studies with synchrotron radiation at DESY is shown in Fig.2[35]. The synchrotron radiation is monochromatized with a channelcut crystal. Usually Ge and Si crystals with surfaces parallel to {111} or {220} are used. The {111} structure factor eliminates second order reflection thus reduces the problem of higher order reflections. The monochromatic radiation is monitored by ionization chambers. The signals of the chambers are amplified by fast current amplifiers and converted to pulse trains the frequencies of which are proportional to the output voltages of the amplifiers. The number of pulses integrated within a preset time

are stored in a computer. The computer controls the angular setting of the goniometer and the position of the table onto which ionization chamber and sample are mounted.

3. Experimental results and evaluation of bond lengths

For simplicity, we will consider only K-edge EXAFS in the following. The absorption coefficient can then be expressed as

$$(1) \qquad \mu = \mu_{0K}\,(1+\chi) + \mu_{LM}$$

Here μ_{0K} and μ_{LM} are monotonous absorption coefficients due to excitation of K-shell electrons (μ_{0K}) and weaker bound electrons (μ_{LM}). Structural informations i.e. bond lengths and coordination numbers can be extracted from χ. The generally adopted dependence of the fine structure on the wave number k of the photoelectrons is given by[4-6]

$$(2) \qquad \chi(k) = -\frac{1}{k}\sum_i A_i(k)\,\sin(\varphi_i(k))$$

with

$$(3) \qquad A_i(k) = (N_i/R_i^2)\,|f_i(\pi,k)|\exp(-2\sigma_i^2 k^2)\exp(-2R_i/L)$$

and

$$(4) \qquad \varphi_i(k) = 2kR_i + \Phi_i(k)$$

Here $|f_i(\pi,k)|$ means the backscattering amplitude of the electrons. The N_i identical scattering atoms at a distance R_i

are grouped together in scattering shells. The first exponential in eq.3 describes the thermal disorder of the atoms with mean square relative displacements σ_i^2 around their average positions. In the last term of eq.3 the damping of the electron wave due to inelastic scattering processes is introduced by a mean free path L of the photoelectrons. The scattering phase $\Phi_i(k) = 2\delta_1 + \arg(f(\pi,k))$ considers the influence of the absorbing (δ_1) and scattering (arg $f(\pi,k)$) atom potentials on the photoelectron wave. The wavenumbers k are calculated from

$$k = (2m/\hbar^2(h\nu - E_0))^{1/2} \quad (5)$$

Here $h\nu$ is the photon energy. The reference energy E_0 in general is unknown. In most cases one-half the step height of the edge is used as E_0 although this can lead to considerable errors in the determination of bond lengths as will be discussed later.

All methods to evaluate bond lengths from EXAFS are based on the general concept of the transferability of phase shifts[3,26,36], i.e. the k-dependences of the scattering phases are characteristic for the absorbing and scattering atom pair. Changes of $\Phi(k)$ due to the chemical environment only play a minor role. Therefore $\Phi(k)$ can be calculated for isolated atoms or extracted from experimental spectra of materials with known geometry and applied to systems of unknown geometrical structure.

To extract information about single scattering shells from experimental spectra, which in general represent superpositions

of contributions from several scattering shells, several approaches have been used:

i) A fit with parametrized envelope functions $A_i(k)$ and phases $\Phi_i(k)$ has been applied to experimental spectra[7,37]. Whereas for simple fine structures, i.e. EXAFS caused by only a single scattering shell, this method yields reliable structural information, the increasing number of parameters in systems with more than one shell limits the applicability of this method.

ii) Experimental spectra have been compared with fine structures calculated from theoretical backscattering amplitudes and phase shifts[38,39]. Backscattering amplitudes $|f(\pi,k)|$ and phases $\delta_1(k)$ and $\arg(f(\pi,k))$ have been calculated individually[40,41]. An arbitrary combination of absorber and backscatterer can be chosen by simply adding the two phase terms. Unfortunately no theoretical phase shifts are available for alkaline (except arg $f(\pi,k)$ of K and Na[39]) and alkaline earth metals and for elements with $Z > 35$.

iii) The most widely applicable method seems to be the Fourier transform technique. The severe problem in this technique is the limited range in k-space from which EXAFS informations can be extracted. The range below $k = 30\ nm^{-1}$, where manybody interactions and density of state effects have to be included in the description of the fine structure, is not adequately described by eq.2, and therefore has to be excluded from the dataprocessing. At high k-values the damping due

to atomic vibrations and due to the decrease of the back-scattering amplitudes limit the range where EXAFS can be observed with significant amplitudes. These facts broaden the structures in real space and limit the spatial resolution considerably. Nevertheless the Fouriertransform yields a radial structure function which can serve as a first survey of the geometrical structure. As an example Fig.3a shows the absorption spectrum of MnO_2 [14]. From this spectrum the fine structure $\chi(k)$ (Fig.3b) has been extracted by removing the monotonous contributions $/u_{oK}$ and $/u_{LM}$. The background $/u_{LM}$ has been approximated by[42]

$$/u_{LM} = a(h\nu)^{-3} + b(h\nu)^{-4} \tag{6}$$

where a and b are obtained from a fit of $/u$ with eq.6 below the edge. The K-shell contribution $/u_{oK}$ has been fitted by a polynomial of second degree in k. The complex Fouriertransform has been calculated by

$$F(r) = \frac{1}{\sqrt{2\pi}} \int_{k_{min}}^{k_{max}} \chi(k) W(k) k^3 e^{2ikr} d(2k) \tag{7}$$

Here k^3 compensates the rapid decrease of $\chi(k)$ at large k-values. The choice of the window function W(k) depends on the spectral distribution of the amplitude functions $A_i(k)$. Generally an abrupt termination at k_{min} and less severe at k_{max} leads to considerable side lobes in F(r). Different functions W(k) have been used which smooth $\chi(k)$ at the boundaries of the transformed range (Gaussian, convolution of square window with

Gaussian)[15,26,43]. The magnitude of F(r) of MnO_2 (Fig.3c) calculated with a Gaussian window function shows three well separated maxima which are caused by the first scattering shells. The structure below 0.1 nm may be due to an incomplete subtraction of background. An atomic origin of such a structure in EXAFS has been discussed by Holland et al[44]. The scattering of photoelectrons by the potentials of the absorbing atom yields long wavelength oscillations in k-space which show up as peaks small r-values in real space. Compared to the true distances the peaks in $|F(r)|$ are shifted due to the k-dependent parts of the scattering phases. Several approaches have been made to extract bond lengths from radial structure functions.

i) In the simplest approach the scattering phases are assumed to be linear functions of k. Then the shift of the peaks in $|F(r)|$ can be simply derived from a reference material of known geometry. For not too heavy atoms this assumption leads to bond lengths with accuracies up to 0.002 nm. For heavy atoms the phases show a considerable nonlinear k-dependence[45]. In these cases the peak shift depends on the k-range under investigation and the weighting with different window functions so that more detailed analysis of the data is necessary.

ii) A refined analysis of EXAFS in real space has been used by Hayes et al[15]. The complex Fouriertransform of a single scattering shell, a peak function, is generated from EXAFS of a structurally known reference sample. The Fouriertransform of EXAFS of the unknown material is then fitted by a linear

combination of peak functions allowing a variation of peak positions and widths.

iii) A third approach is the combination of the Fouriertransform technique and the interpretation of EXAFS in k-space[26,47]. The separation of different terms in eq.2 can be accomplished by a backtransform of a limited range of F(r) to k-space:

$$\overline{\chi}_i(k) = 2(W(k)k^3\sqrt{2\pi})^{-1}\int_{r_1}^{r_2} F(r)e^{-2ikr}dr \qquad (8)$$

From the amplitude function $A_i(k)$, the total phase $\varphi_i(k)$, and, together with a known bondlength, the scattering phase $\Phi_i(k)$ can be calculated. Once $\Phi_i(k)$ is determined, the bond length R_i of an unknown material containing the same atom pairs can be determined simply by

$$R_i = (\varphi_i(k) - \Phi_i(k))/2k \qquad (9)$$

In general the R_i determined in this way show a considerable k-dependence. Deviations of R_i from a constant value due to termination effects of the Fouriertransform are confined to small ranges at the boundaries. A k-dependence of R_i over the whole k-range can appear due to differences in the reference energies E_o. It has been shown by Martens et al[26] that reliable bond lengths can be determined by varying E_o in a way to obtain constant R_i in the whole k-range. This procedure is demonstrated for the first scattering shell of Cu in Fig.4. The solid line was obtained by applying the theoretical phase of Ashley and Doniach[5] fixing the experimental E_o at the inflection point of the K-edge. The strong k-dependence can be

almost completely removed by fixing the zero of kinetic energy 16 eV below the edge. The result of R = 0.2554 ± 0.001 nm is in close agreement to the value of 0.2556 nm determined by X-ray diffraction[46]. The resulting deviation below $40nm^{-1}$ are due to uncertainties in the theoretical phases and due to termination effects in the Fouriertransform.

Differences of bond lengths of the same atompairs in different chemical compounds can be extracted from experimental spectra with high precision. A backtransform of two isolated peaks in |F(r)| for two different materials A and B produced by the same kind of atom pairs allows the calculation of

$$\Delta R = (\varphi_A(k) - \varphi_B(k))/2k \qquad (10)$$

This has been demonstrated for the nearest neighbour distances in MnO_2 and MnO_4^- in aqueous solutions[14]. The fine structure $\chi(k)$ and the Fouriertransform |F(r)| of MnO_4^- are shown in Fig.5 In both cases the range in real space as indicated by bars in Fig. 3c and 5d has been transformed back to k space and Δ R has been calculated. Comparing MnO_2 with MnO_4^- the Mn-O bond length decreases by 0.0231 nm. The deviation of Δ R from a constant value by less than 0.0003 nm indicates the accuracies which can be achieved for bond lengths determined from EXAFS.

4. Beats in EXAFS

Differences of bond lengths of close lying shells in the same compound can be extracted from a beating in EXAFS[47]. The superposition of contributions from two shells in eq.2 can be expressed as

$$\chi(k) = -\frac{1}{k}\bar{A}(k)\sin(\bar{\varphi}(k)) \tag{11}$$

with

$$\bar{A}(k) = A_1(k)(1 + C^2 + 2C\cos(2k\Delta R))^{1/2} \tag{12}$$

$$\bar{\varphi}(k) = 2k\bar{R} + \Phi(k) + \tan^{-1}\left\{\frac{C-1}{C+1}\tan(k\Delta R)\right\} = 2k\bar{R} + \bar{\Phi}(k) \tag{13}$$

Here $C = A_2/A_1$, ΔR is the difference in bond lengths of the two shells and $\bar{R}$ the average bond length. The extreme values of $\bar{A}(k)/A_1(k)$ and inflection points of $\bar{\varphi} - \Phi$ are simply determined by $k_E = (n\pi)/(2\Delta R)$.

The effect of this superposition is shown on a synthetic EXAFS spectrum with two shells at a distance of $R_1 = 0.16$ nm and $R_2 = 0.19$ nm from the absorbing atom using a phase $\Phi(k) = 3.11 - 0.6\,k + 0.012\,k^2$ and a k-dependence of the envelope function proportional to $k^{-1.8}$. The spectrum for $A_1 = A_2$ is shown in Fig.6a. Using a Gaussian window this spectrum was transformed to real space. The magnitude of the Fouriertransform for this case is shown in Fig.6b. From this figure a value for the difference in bond length of roughly 0.04 nm can be deduced, which shows the large error in comparison to the

assumed difference of 0.03 nm. Radial distribution functions produced by shells occupied with unequal numbers of atoms do not show structures from which the distances can be determined safely. In order to evaluate distances from the average envelope function and phase the radial distribution functions have been transformed back to k - space for both shells simultaneously. $\bar{A}(k)$ and $\bar{\Phi}(k)$ have been calculated. The k-dependence of envelope and phase are shown in Fig.6c and d for four different values of C. In this Figure they are also compared with the envelope and phase of a single shell. In all cases the modulation of $\bar{A}(k)$ can be seen. From the minimum in $\bar{A}(k)$ for $C = 1$ a value $\Delta R = 0.0298$ nm has been calculated which is in excellent agreement with the starting value. For shells with $C \neq 1$ the minimum is slightly shifted by the slope of the amplitude $A_1(k)$. But even for these cases the errors in ΔR are less than 0.002 nm while a determination of ΔR directly from the radial structure function is impossible.

The phases (Fig.6d) show the expected inflection points. Their k values coincide with the extreme values of the envelope function and therefore yield an independent criterion for the determination of ΔR. The accuracy is mainly determined by the error of reading the k value of the inflection point and the deviation from a linear shape of the phase in k. It should be noted that for $0.5 < C < 1.5$ the average phase $\bar{\Phi}(k)$ follows closely the phase $\Phi(k)$ of the single shell around the inflection points with even n values. With $\Phi(k)$ the average distance

$\bar{R}$ of two shells can be calculated. The change of the slope of $\bar{\Phi}(k)$ allows a determination of C. For $C > 1$ the phase rises to positive values while for $C < 1$ a decrease to negative values around the inflection points.

This method has been successfully applied to the determination of differences of Cu-O bond lengths in CuO[47] and Mn-O bond lengths in $KMnO_4$[14]. The normalized spectrum of $KMnO_4$ at the Mn K-edge is included in Fig.5 . The splitting ΔR of the shells in $KMnO_4$ as well as the difference $\Delta\bar{R}$ of MnO_4^- bond length and average $KMnO_4$ bond length have been obtained from the backtransform over the ranges indicated in Fig.5.

Using eq.7 and 12 one obtains

$$14) \qquad D(k) = (\varphi_{MnO_4^-} - \varphi_{KMnO_4})/2k$$

$$= \Delta\bar{R} + (2k)^{-1}\tan^{-1}\left\{\frac{C-1}{C+1}\tan(k\Delta R)\right\}$$

The experimental D(k) has been fitted with eq.14. The fit yields $\Delta\bar{R} = (0.0047 \pm 0.0003)$ nm, $\Delta R = (0.0125 \pm 0.0003)$ nm and $C = 0.28$. Compared to MnO_4^- in $KMnO_4$ the bond length of one oxygen atom has increased by 0.0110 nm and the bond lengths of three atoms have decreased by 0.0015 nm.

5. Non-symmetric pair distribution function

The fact that the assumption of a symmetric pair distribution and the approximation of $\chi(k)$ by eq.2 can lead to substantial errors in the determination of bond lengths has been recently pointed out by Eisenberger and Brown[48]. They have shown that changes of the nearest neighbour distances with temperature of zinc using eq.1 have been in error up to 0.14 Å compared to values determined by thermal expansion measurements. For arbitrary pair distributions $g_i(R)$, EXAFS has to be expressed by

$$(15) \qquad \chi(k) = \sum_i \frac{|f_i(\pi,k)|}{k} e^{-2\bar{R}_i/L} \int_0^\infty \frac{g(R_i)}{R_i^2} \sin(2kR_i + \Phi)\,dR_i$$

Due to asymmetries in $g(R_i)$ and due to the additional asymmetry introduced by $1/R_i^2$ eq.1 must be replaced by

$$(16) \qquad \chi(k) = \sum_i \frac{|f_i(\pi,k)|}{k} e^{-2\bar{R}_i/L} \left\{U_i^2+S_i^2\right\}^{1/2} \sin(2k\bar{R}_i + \Phi + \tan^{-1}\frac{U_i}{S_i})$$

where U(k) and S(k) are the asymmetric and symmetric components of $g(R)/R^2$. The most severe problem for the determination of bond lengths arises from the additional k dependent phase term $\tan^{-1}\frac{U(k)}{S(k)}$. It contains detailed information about the radial pair distribution which in general is unknown. Eisenberger and Brown have approximated this phase term by $-ak-bk^3$ with a and b proportional to the temperature dependent second and third moments of g(R) respectively. With these assumptions they improved their bond lengths of zinc to accuracies better than

0.001 nm. Most of these problems are removed when experimental phases are transferred between systems with equivalent pair distribution functions or if $\tan^{-1}(U(k)/S(k))$ is small. Nevertheless this fact imposes severe limitations on the determination of high accuracy bond lengths.

6. Conclusion

Improvements in the data evaluation by means of the Fourier-transform technique together with the utilization of synchrotron radiation have raised the accuracies of bond lengths determined from EXAFS to 10^{-3} - 10^{-4} nm. These values bear comparison with data derived from X-ray diffraction on crystalline materials.

The methods described here have been demonstrated on spectra obtained in transmission experiments. A substantial expansion of the range of application of EXAFS will emanate from additional experimental techniques cited in the introduction. The description of these techniques is beyond the scope of this paper.

Acknowledgements

This work was supported by the Bundesministerium für Forschung und Technologie (BMFT), the Deutsches Elektronen-Synchrotron (DESY), and the Deutsche Forschungsgemeinschaft (DFG). I thank G. Martens, Dr. N. Schwentner, G. Tolkiehn, and A. Werner for many stimulating discussions, Prof. F. C. Brown for a critical reading of the manuscript, and Prof. R. Haensel for his personal support.

References

1.) L.V. Azaroff, Rev.Mod.Phys.35 (1958) 1012

2.) F.W. Lytle, D.E. Sayers, and E.A. Stern, Phys.Rev.B11 (1975) 4825

3.) E.A. Stern, D.E. Sayers, and F.W. Lytle, Phys.Rev.B11 (1975) 4836

4.) E.A. Stern, Phys.Rev.B10 (1974) 3027

5.) C.A. Ashley and S. Doniach, Phys.Rev.B11 (1975) 1279

6.) P.A. Lee and J.B. Pendry, Phys.Rev.B11 (1975) 2795

7.) R.G. Shulman, P. Eisenberger, W.E. Blumberg, and N.A. Stombauch, Proc.Nat.Acad.Sci. USA 72, (1975) 4003

8.) D.E. Sayers, E.A. Stern, and J.R. Herriot, J.Chem.Phys.64 (1976) 427

9.) B. Bunker and E.A. Stern, Biophys.J.19 (1977) 253

10.) D.E. Sayers, F.W. Lytle, M. Weissbluth, and P. Pianetta, J.Chem.Phys.62 (1975) 2514

11.) P. Eisenberger and B.M. Kincaid, Chem.Phys.Letters 36 (1975) 134

12.) A. Fontaine, P. Lagarde, D. Raoux, M.P. Fontana, G. Maisano, P. Migliardo, and F. Wanderlingh, to be published in Phys.Rev.Letters

13.) D.R. Sandstrom, H.W. Dodgen, and F.W. Lytle, J.Chem.Phys.67 (1977) 473

14.) P. Rabe, G. Tolkiehn, and A. Werner, to be published in J.Phys.C

15.) T.M. Hayes, P.N. Sen, and S.H. Hunter, J.Phys.C 9 (1976) 4357

16.) D.E. Sayers, E.A. Stern, and F.W. Lytle, Phys.Rev.Letters 27 (1971) 1204

17.) J.C. Knights, T.M.Hayes, and J.C. Mikkelsen, Jr., Phys.Rev.Letters 39 (1977) 712

18.) D.E. Sayers, E.A. Stern, and F.W. Lytle, Phys.Rev.Letters 35 (1975) 584

19.) R.F. Pettifer and P.W.Mc.Millan, Phil.Mag. 35 (1977) 871

20.) E.D. Crozier, F.W. Lytle, D.E. Sayers, and E.A. Stern, Can.J.Chem. 55 (1977) 1968

21.) G.S. Brown, L.R. Testardi, J.H. Wernick, A.B. Hallak, and T.H. Geballe, Solid State Communications 23 (1977) 845

22.) P. Rabe, G. Tolkiehn, and A. Werner, to be published

23.) G.S. Brown, P. Eisenberger, and P. Schmidt, Solid State Communications 24 (1977) 201

24.) J.B. Boyce, T.M. Hayes, W. Stutius, and J.C. Mikkelsen, Phys.Rev.Letters 38 (1977) 1362

25.) S.M. Heald and E.A. Stern, Phys.Rev.B16 (1977) 5549

26.) G. Martens, P. Rabe, N. Schwentner, and A. Werner, Phys.Rev.B17 (1978) 1481

27.) P. Rabe, G. Tolkiehn, and A. Werner, to be published

28.) J. Jaklevic, J.A. Kirby, M.P. Klein, A.S. Robertson, G. S. Brown, and P. Eisenberger, Solid State Communications 23 (1977) 679

29.) A. Bianconi, D. Jackson, and K. Monohan,
Phys.Rev.B17 (1978) 2021

30.) P.H. Citrin, P. Eisenberger, and R.C. Hewitt,
Phys.Rev.Letters 41 (1978) 309

31.) G. Martens, P. Rabe, N. Schwentner, and A. Werner,
J.Phys.C11 (1978) 3125

32.) P.A. Lee, Phys.Rev.B13 (1976) 5261

33.) J.B. Hastings, B.M. Kincaid, and P. Eisenberger
Nucl.Inst. and Methods 152 (1978) 167

34.) J.A. Del Cueto and N.J. Shevchik, J.Phys.E11 (1978)

35.) P. Rabe, G. Tolkiehn, and A. Werner, to be published

36.) P. H. Citrin, P. Eisenberger, and B.M. Kincaid,
Phys.Rev.Letters 36 (1976) 1346

37.) S.P. Cramer, T.K. Eccles, F. Kutzler, K.O. Hodgson,
and S. Doniach, J.Am.Chem.Soc.98 (1976) 8059

38.) P.A. Lee and G. Beni, Phys.Rev.B15 (1977) 2862

39.) P. Lagarde, Phys.Rev.B14 (1976) 741

40.) P.A. Lee, Boon-Keng Teo, and A.L. Simons,
J.Am.Chem.Soc.99 (1977) 3856

41.) Boon-Keng Teo, P.A. Lee, A.L. Simons, P. Eisenberger,
and B.M. Kincaid, J.Am.Chem.Soc.99 (1977) 3854

42.) International Tables for X-Ray Crystallography III
edited by K. Konsdale et al (Kynoch, Birmingham,
England, (1962), Sec. 3.2

43.) S.J. Gurman and J.B. Pendry,
Solid State Communications 20 (1976) 287

44.) B.W. Holland, J.B. Pendry, R.F. Pettifer, and
J. Bordas, J.Phys.C11 (1978) 633

45.) P. Rabe, G. Tolkiehn, and A. Werner, submitted to
J.Phys.C

46.) R.W.G. Wyckoff, Crystal Structures (Interscience,
New York 1968)

47.) G. Martens, P. Rabe, N. Schwentner, and A. Werner
Phys.Rev.Letters 39 (1977) 1411

48.) P. Eisenberger and G.S. Brown, to be published in
Phys.Rev.Letters

Figure captions

Fig. 1: Comparison of intensities of an X-ray tube with Cu anode (45 kV, 50 mA, 20^{o} take off angle, 1 mm Be window) and the synchrotron radiation of DESY (10 mA) for various usable solid angles.

Fig. 2: Experimental set up at DESY (C current amplifier, CR crystal, GO goniometer, IC ionization chamber, LS lead slit, LT lifting table, RC reference counter, S sample, SC signal counter, VF voltage to frequency converter).

Fig. 3: Absorption coefficient (a), EXAFS (b), and magnitude of the Fouriertransform (c) of MnO_2 at the Mn K-edge.

Fig. 4: Determination of bond length of the first scattering shell of Cu with theoretical phase shift of ref.5.
a) E_o fixed at the inflection point of the edge.
b) E_o shifted 16 eV below the edge.

Fig. 5: EXAFS and magnitude of the Fouriertransform of $KMnO_4$ and MnO_4^-(aq) at the Mn K-edge.

Fig. 6: EXAFS of two close lying shells with equal coordination numbers and ΔR = 0.03 nm (a). The resulting magnitude of the Fouriertransform (b), the modulation of the envelope function (c), and the scattering phases are shown. C is the ratio of the envelope function.

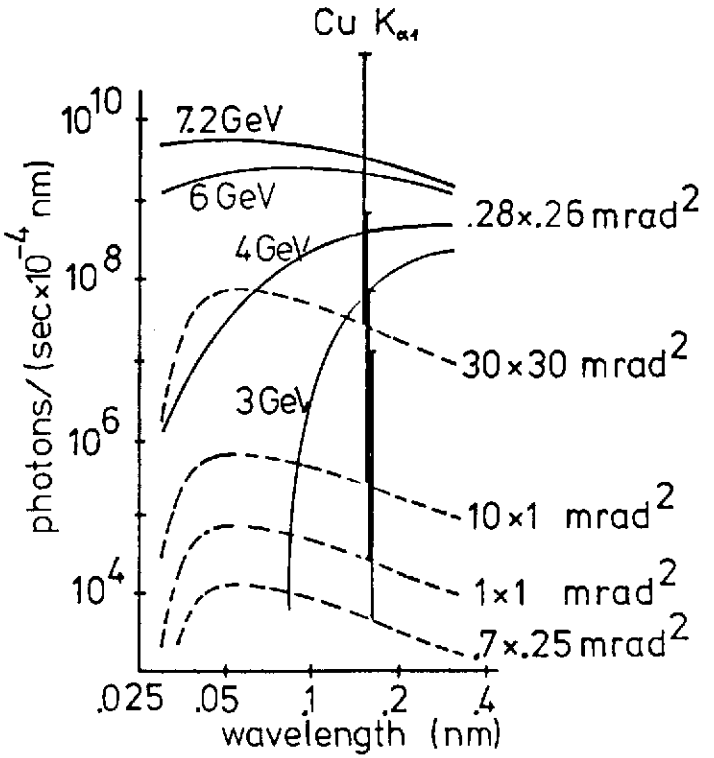

Fig. 1

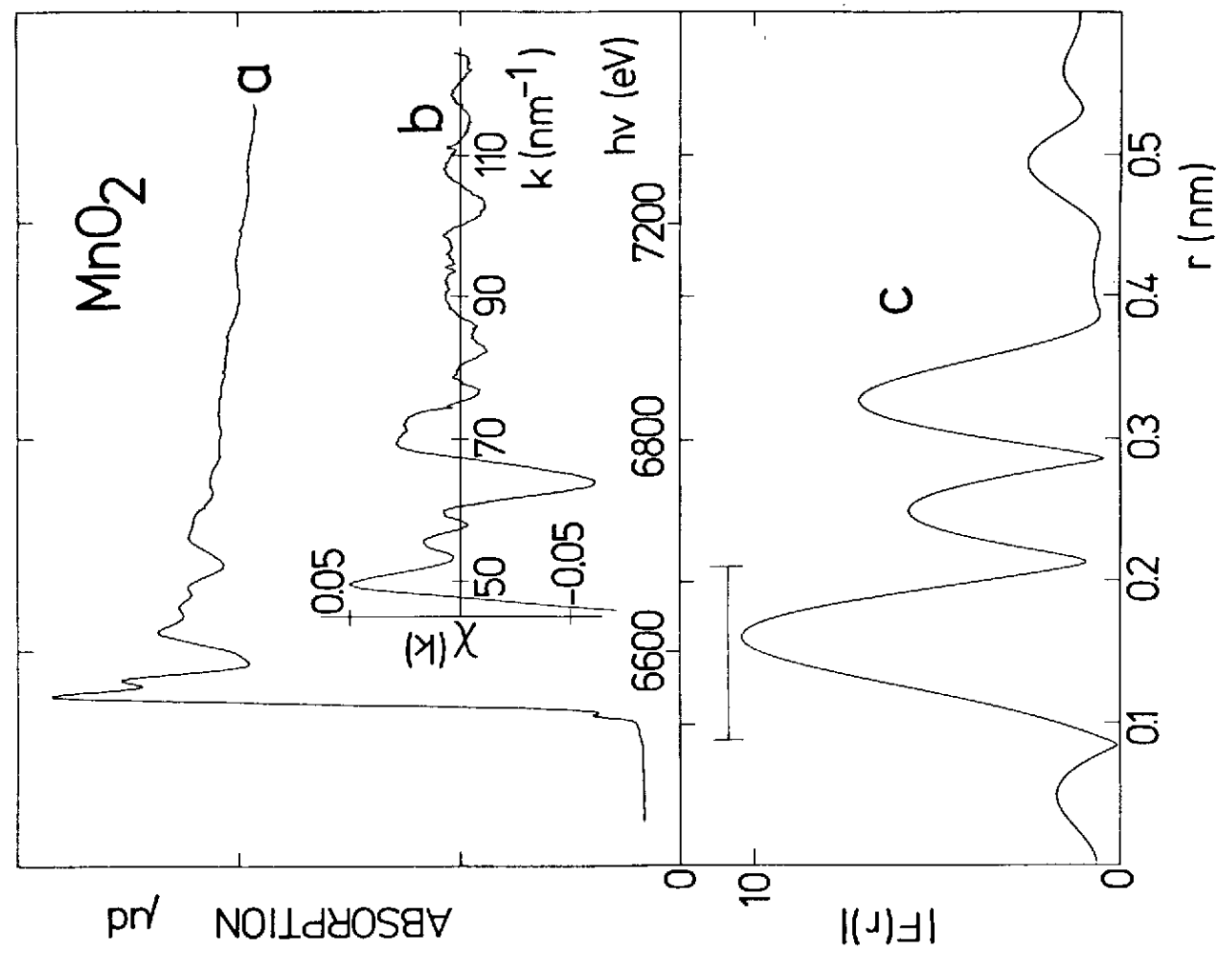
MnO2
a
b
c
k (nm⁻¹)
hν (eV)
r (nm)
χ(k)
ABSORPTION
|F(r)|

Fig. 3

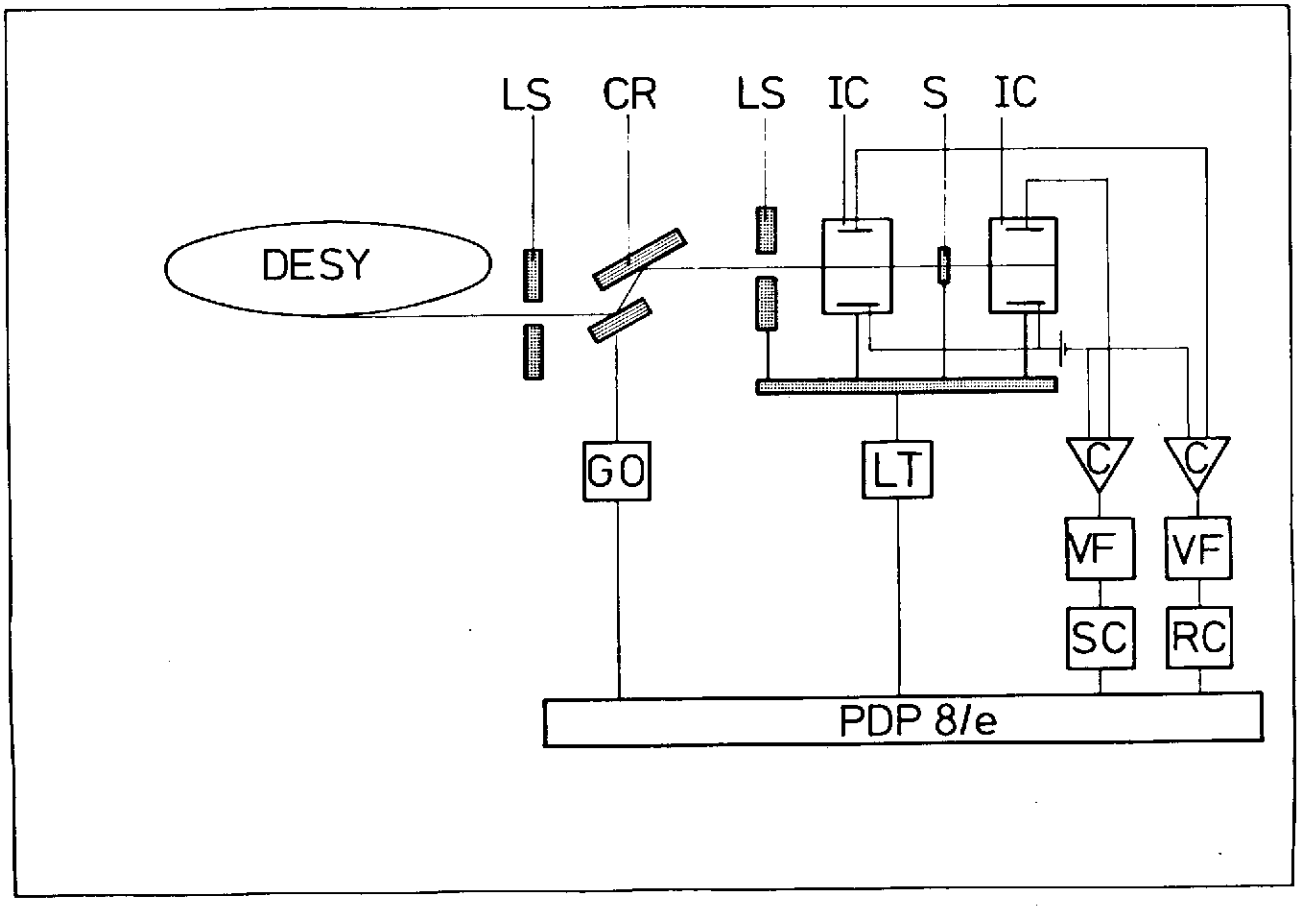
LS
CR
LS
IC
S
IC
DESY
GO
LT
C
C
VF
VF
SC
RC
PDP 8/e

Fig. 2

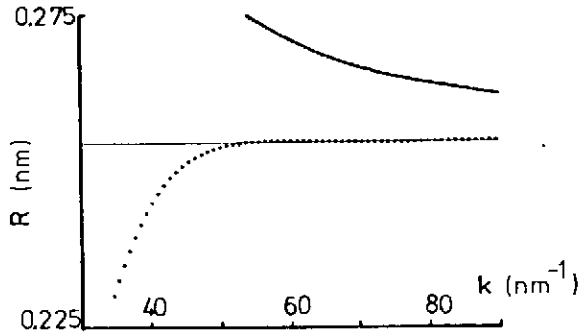
0.275
R (nm)
0.225
40
60
80
k (nm^{-1})

Fig. 4

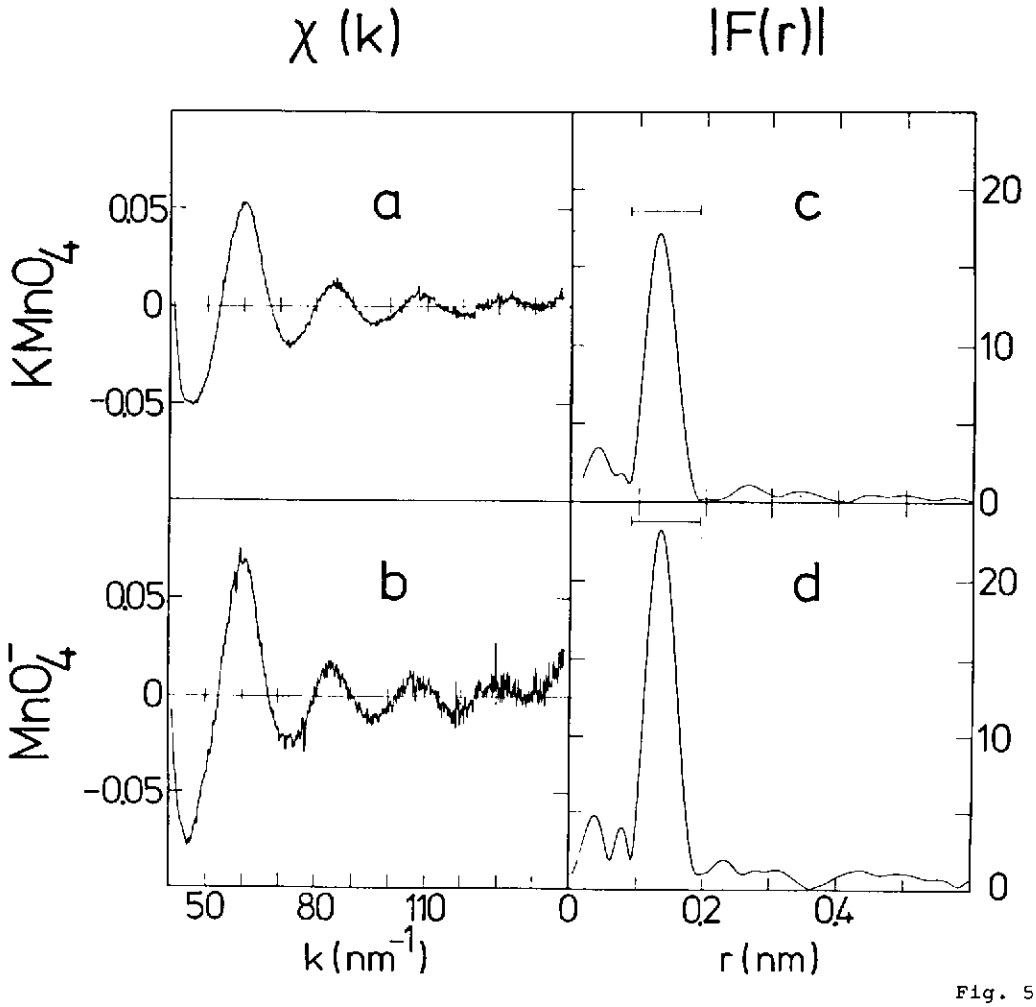
χ (k)
|F(r)|
KMnO$_4$
MnO$_4^-$
a
b
c
d
0.05
0
-0.05
20
10
50
80
110
0
0.2
0.4
k (nm^{-1})
r (nm)

Fig. 5

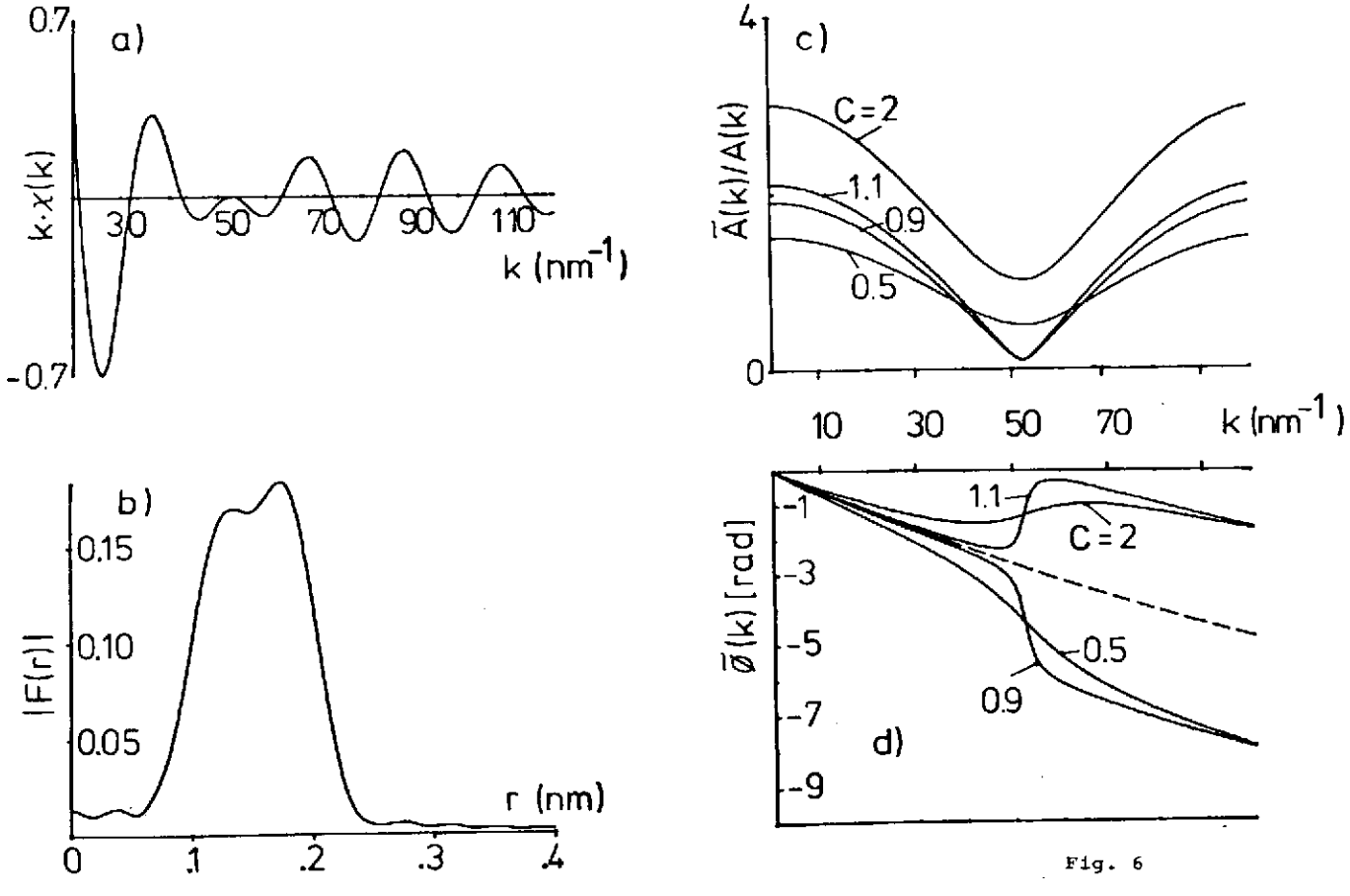
a)
0.7
-0.7
k·χ(k)
30
50
70
90
110
k (nm⁻¹)
b)
|F(r)|
0.15
0.10
0.05
r (nm)
0
.1
.2
.3
.4
c)
4
0
Ã(k)/A(k)
C=2
1.1
0.9
0.5
10
30
50
70
k (nm⁻¹)
d)
ø̃(k) [rad]
-1
-3
-5
-7
-9
1.1
C=2
0.5
0.9

Fig. 6